Fuel 356 (2024) 129529

Contents lists available at ScienceDirect

Fuel

journal homepage: www.elsevier.com/locate/fuel

Full Length Article

Sensitivity analysis and process optimization for biomass processing in an integrated gasifier-solid oxide fuel cell system

Hafiz Hamza Faheem [a], Ben Britt [a], Mateus Rocha [b], Shou-Han Zhou [a], Chao'en Li [c,*], Weiwei Cai [d], Liyuan Fan [a,*]

[a] College of Science and Engineering, James Cook University, 1 James Cook Drive, Townsville, QLD 4811, Australia
[b] Federal University of Itajubá (UNIFEI), BPS Avenue, N° 1303, Itajubá, Minas Gerais State Postal Office Box: 37500-903, Brazil
[c] CSIRO Energy, 71 Normanby Road, Clayton North, Victoria 3169, Australia
[d] Sustainable Energy Laboratory, Faculty of Materials Science and Chemistry, China University of Geosciences, Wuhan 430074, Hubei, China

ARTICLE INFO

Keywords:
Solid oxide fuel cell
Electricity and hydrogen cogeneration
Biomass to hydrogen
Process optimization

ABSTRACT

Hydrogen (H_2) production from biomass is always attractive due to its carbon–neutral nature. However, the high energy requirement in biomass gasification and the processing of synthesis gas (syngas) has become the primary concern of the application of this technique. The combined gasifier-solid oxide fuel cell (SOFC) system shows promising potential for significant energy efficiency improvement. However, there is still space to optimize the performance of such combined systems. A novel zero-dimensional (0D) mass-transfer-based model was developed to find the optimal operating parameters for H_2 production and to maximize the power density. Coal, sugarcane bagasse, and marine algae were used as feeds to analyze the effects of relevant parameters. A sensitivity analysis of the operational conditions was undertaken to better understand the characteristic trends associated with the maximum power and H_2 production. This work optimized the conditions respected with the power density. It was found that the highest power density could be achieved by manipulating operating variables. It is concluded that marine algae have the highest power output but the lowest system efficiency due to high moisture and ash content. Coal produces low power output than biomasses. Hence, sugarcane bagasse is the most efficient feedstock for integrated gasifier-SOFC systems.

1. Introduction

Increasing energy consumption over the last century due to the industrial and population growth has caused an increase in energy demand. The usage of fossil-based energy leads to a large number of suspended particles and Greenhouse Gas (GHG) emissions, which impact global warming significantly [1–3]. As global warming has become a major concern for the population throughout the past years, the Kyoto protocol (2005) and Paris agreement (2015) make efforts to constrain its effect to a maximum global temperature change of 2 °C [4]. As a result, energy production is forced to shift to renewable and sustainable energy resources to mitigate this issue and assist the economic stability of the world. Many states in United States of America (USA) have a long-term goal to achieve a 100% clean or renewable electricity-supported grid by 2050, and New South Wales (NSW) in Australia also has a long-term plan to achieve net-zero GHG emissions by 2050 [5,6].

Alternative fuels, such as hydrogen (H_2), have been considered promising to solve the concerns of energy security and sustainability [2,3,6]. H_2 can be completely sustainable if the needed energy for its production is supplied from renewable sources [7,8]. As a carbon–neutral source, biomass has less environmental impact on H_2 production for power generation than fossil fuels. H_2 generated from biomass is considered green H_2 as the released CO_2 during the H_2 generation process almost gets compensated by the amount of absorbed CO_2 while biomass grows. Biomass conversion technologies vary in system efficiency, services provided, and market demand as designed for different end-products [2]. Therefore, developing new methods to control biomass decomposition is an alternative for cleaner energy production. A study supported by the European Fuel Cells and Hydrogen Joint Undertaking (FCH-JU) on the green H_2 analyzed the possible pathways to produce H_2 from renewable energy sources from a technical and economic point of view. The less expensive and promising way for green H_2 production is biomass gasification and biogas reforming processes [9]. Gasification is a thermal decomposition process of solid or liquid organic materials into H_2–rich bio-synthesis gas (bio-syngas) in the presence of

* Corresponding authors.
E-mail address: liyuan.fan@jcu.edu.au (L. Fan).

https://doi.org/10.1016/j.fuel.2023.129529
Received 3 May 2023; Received in revised form 15 June 2023; Accepted 14 August 2023
Available online 26 August 2023

Nomenclature

E	Activation energy (J/mol)
F	Faraday constant (C/mol)
G	Gibbs free energy (J/mol)
j	Current density (A/cm^2)
K	Permeability (–)
P	Pressure (bar)
P_i	Partial pressure of ith component (bar)
Q	Total energy (kW)
R_{tot}	Total electrical resistance (Ω)
R	Universal gas constant (J mol^{-1} K^{-1})
SC_a	Actual steam-to-carbon ratio
SC_e	External steam-to-carbon ratio
T	Temperature (°C)
V	Voltage (V)
x_i	Molar fraction of ith components (-)
y_i	Mass fraction of ith component (-)

Greek Letters

$\eta_{overall}$	System efficiency

Acronym

0D	Zero dimensional
1D	One dimensional
3D	Three dimensional
BRM	Bi-reforming of methane
CFD	Computational fluid dynamics
DMR	Dry methane reforming
DEN	Denominator
GHG	Greenhouse gas
LHV	Lower heating value
MSR	Methane steam reforming
GDC	Gadolinium-doped ceria
PFR	Plug flow reactor
PL	Power law
POM	Partial oxidation of methane
RMS	Root mean square
SA	Surface area
SB	Steam to biomass
SC	Steam to carbon
SOFC	Solid oxide fuel cell
SRK	Soave Redlich Kwong
TPB	Triple phase boundary
WGS	Water-gas shift

gasification agents [10]. The produced bio-syngas is a mixture of hydrogen (H_2), methane (CH_4), carbon monoxide (CO), and carbon dioxide (CO_2), which can be widely used in several industries, such as H_2 production, combined heat and power (CHP) generation, and synthesis for chemical production. Biomass gasification can produce H_2-rich bio-syngas with a thermal efficiency of up to 57–77% [11,12]. The recent and advanced approaches for H_2 production from bio-syngas are methane steam reforming (MSR), dry methane reforming (DMR), bi-reforming of methane (BRM), and partial oxidation of methane (POM). However, both biomass gasification and bio-syngas reforming are highly energy-demanded processes. Therefore, a sustainable and stable energy supply system should always be considered for the process design [13–15].

The solid oxide fuel cell (SOFC) is one of the most promising technologies for power production. It has also shown promise in its energy efficiency and flexibility as a power producer. SOFC has been known for over 20 years, where the effects of material, temperature, current, feed, flow rate, and experimental parameters on the SOFC and its efficiency have been investigated vastly [16]. A typical lifetime of a stationary SOFC is 40,000 h. In principle, SOFCs can operate on any combustible fuel capable of reacting with O^{2-} coming through the electrolyte. This makes the internal reforming in SOFCs a more thermal efficient process. An SOFC is operated as a catalytic electrochemical facilitator to provide reasonable control and optimization over H_2 and energy production at 800–1000 °C utilizing any fuel containing hydrocarbons and is generally mixed with various reforming agents [17]. SOFC produces heat and electricity by converting the chemical energy of the fuel through MSR, water–gas shift (WGS), and half-electrochemical reactions at the triple phase boundary (TPB) [18]. Therefore, the gasification process can be combined with SOFC to become a flexible power-H_2 production system that offers one of the highest efficiencies in energy production [11,19].

The syngas produced from biomass gasification contains impurities such as tar, sulfur, halogens, and alkali metal [20]. As impurities can have both reversible and irreversible effects on SOFC performance, the presence of these impurities limits the practical feasibility of integrated gasifier SOFC systems. The gas cleaning units may be required to avoid this detrimental effect on SOFC anodes. For instance, the presence of heavier hydrocarbon in tar can cause carbon deposition on the anode due to thermal degradation and can block the active sites for the reactants. The detrimental effect of tar components on SOFC performance is widely reported in the literature [21–26]. Tar can be removed using physical methods and thermos-chemical transformation technologies. In the prior method, tar components are removed using a cyclone, scrubber, or filter, while tar is converted into syngas through a catalyst or high-temperature conversion [27,28].

Sulphur compounds are well-known impurity that causes deleterious effects on SOFC performance. Sulphur can have both reversible and irreversible effects on SOFC performance. High sulphur concentration poisoning consists of two steps: the reversible voltage firstly falls till the metastable cell voltage, then the irreversible voltage degradation may lead to fatal performance loss [29,30]. The mechanism of sulphur poisoning and safe concentration limit depends on the anode material. Nickel-based catalysts are more susceptible to sulphur poisoning. The low concentration of sulphur (<2 ppm) can cause performance loss [31]. Moreover, some catalyst materials are immune to sulphur poisoning. Lanthanum strontium vanadate and titanate (LSV and LST)-based anodes are unaffected by sulphur [32,33]. The later anode showed power enhancement despite increased polarization resistance when 0.5% H_2S was present in the fuel gas [33]. The sulphur concentration in syngas can be reduced using sorption techniques and dolomite, limestone, and zinc-based sorption materials give promising results [34].

Halogens such as HCl are other noticeable impurities. However, they do not have a severe impact on SOFC performance. Papurello et al. [35] concluded that the HCl concentration up to 40 ppm does not affect the performance of SOFC. The HCl in syngas is removed using alkali-based sorbents, mainly sodium and potassium [36].

The use of syngas from biomass gasification in SOFC is still in an early stage of application, and experiments on integrated biomass gasification and SOFC systems are still limited. The performances of these systems have been examined from a practical point of view by only a few studies [37]. Therefore, it is crucial to model the integrated gasifier-SOFC system to find the optimal parameters. Process limitations and undesirable and hazardous operational conditions can be predicted and determined using simulation before the real experimental work [38]. The use of syngas in SOFC has been explored in literature, including the combined gasifier-SOFC system. Simulation and

optimization of complex processes via software simulators such as Aspen Hysys® and Aspen Plus® (Aspen Tech), ChemCAD® (Chemstations), COCO/COFE® (AmsterCHEM), Cycle-Tempo (Asimptote), DWSIM® (Open Source CAPE-OPEN process simulator), gPROMS® (Siemens Process Systems Engineering), ProSimPlus (ProSim), SimSci PRO/II® (SimSci/Invensys), and UniSim® (Honeywell), which can perform material and energy balances, and equipment sizing of many chemical processes [39].

A variety of 0, 1, 2, and 3-dimensional simulations have been conducted to find trends in gas concentration, voltage (V), and feed utilization throughout the SOFC anode [40]. In addition, the performance indicator of electrical efficiency has been explored with variations in gasifier conditions using a Gibbs free energy SOFC module [41]. Models using Aspen Plus® that include gasifier and SOFC systems mainly utilized a zero-dimensional (0D) Gibbs free energy solution method. However, little work has been published on the optimization of performance indicators other than the relationship between the current and power densities. Therefore, the main objective of this work is to develop a combined gasifier-SOFC system to evaluate the influence of the operating parameters on the system performance, including the overall efficiency, hydrogen yield, and power density. To incorporate the direct internal reforming (DIR) of CH_4 and simultaneous electrochemical consumption of H_2, each SOFC is divided into ten equally sized sub-cells. This novel approach introduces electrochemical reactions after each interval and incorporates the effect of water production at the triple phase boundary (TBP) on methane steam reforming (MSR) and water-gas shift (WGS) reaction kinetics in the adjacent sub-cell.

Moreover, the detailed heat integration of the system is carried out by utilizing the excess system heat for high-pressure steam generation. The additional power is generated with the steam, and the steam is recycled to improve the overall system efficiency. Furthermore, the utilization of this model aims to find characteristics relating to different feeds including biomasses and coal, operating conditions, and their effects on performance indicators, eventually leading to the optimal conditions for maximum power density. This work may provide a better understanding of integrated gasifier-SOFC systems for co-producing green power and H_2-rich gas.

2. Process simulation and validation

This research focuses on the simulation of biomass processing in an integrated gasifier-SOFC system using Aspen Plus, where the MSR kinetics will be applied in SOFC to find the optimum conditions for H_2 and power production using the biomass-derived syngas from the gasifier. The first step will utilize an iterative design process to build a model and increase its accuracy within Aspen Plus. The second stage is an experimental approach toward different biomasses to find their respective optimal operating conditions for the given model. The overall process flow diagram of the integrated gasifier-SOFC system is shown in Fig. 1. The Aspen Plus modelling process flowsheet is available in **Supplement**.

The model is based on the following assumptions [42]:

1. Isothermal operation in the gasifier;
2. Pressure drops are neglected;
3. All fuel bound N is converted to NH_3 and S into H_2S;
4. Tar formation is not considered;
5. Heat loss is neglected;
6. Complete conversion of combustibles gases achieved in the burner.

2.1. Gasifier

Generally, both steam and oxygen can be used as oxidizing agents in a gasifier [43,44]. However, steam is used as a gasifier agent to get a higher H_2 yield in this study. Therefore, the following reactions may occur in the gasifier.

$$Boudouard\ reaction: C + CO_2 \leftrightarrow 2CO \quad \text{(R1)}$$

$$Reforming\ of\ char: C + H_2O \rightarrow CO + H_2 \quad \text{(R2)}$$

$$Steam\ methane\ reforming: CH_4 + H_2O \rightarrow CO + 3H_2 \quad \text{(R3)}$$

$$Water-gas\ shift: CO + H_2O \leftrightarrow CO_2 + H_2 \quad \text{(R4)}$$

$$Methanation\ reaction: C + 2H_2 \rightarrow CH_4 \quad \text{(R5)}$$

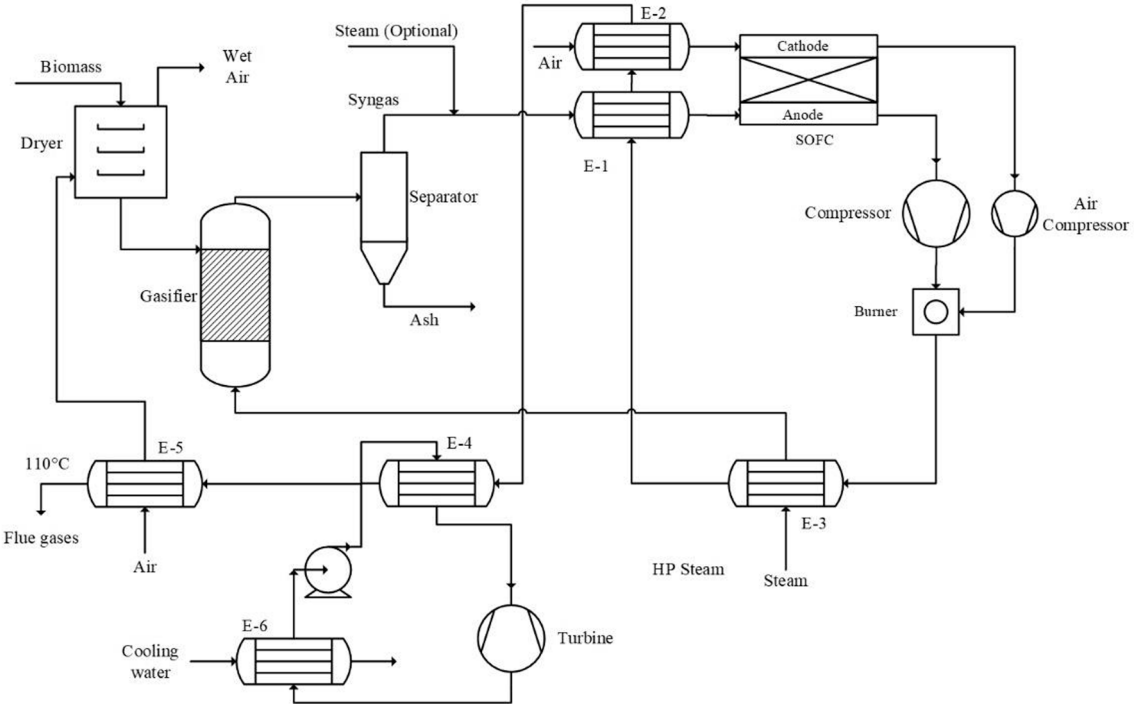

Fig. 1. Process flow diagram of the integrated gasifier-solid oxide fuel cell system.

$$Dry\ reforming: CH_4 + CO_2 \rightarrow 2CO + 2H_2 \quad (R6)$$

The gasification reactions are driven by the equilibrium; hence a Gibbs reactor is chosen as a gasifier. The biomass is represented with a proximate analysis (55.54% volatile, 14.99% fixed carbon, 9.95% moisture and 19.52% ash) and an ultimate analysis (38.43% carbon (C), 2.97% hydrogen (H), 0.49% nitrogen (N), 0.07% sulfur (S) and 36.36% oxygen (O). The gasifier uses 3.6 kg/h of biomass feed rate, steam as a gasifier agent with a 1:1 steam-to-biomass ratio (SB), and a temperature of 750 °C. The simulation results of the gasification section were validated against the experimental results published by Karmakar et al. [45] and are summarized in Table 1.

From Table 1, there is a root mean square (RMS) error of 4.34% between the reference experimental and the model results, which is mainly contributed by the mole percentage of CH_4. The gasifier applied in this model is a homogenous 0D reactor, while the reactor used in experiments is heterogeneous and three-dimensional (3D). Therefore, in the experiment, adequate time may not be provided for the complete conversion of CH_4 by R3, while in the present model, the equilibrium is achieved at a given operating condition. Therefore, the CH_4 percentage is lower, and the H_2 percentage is higher than the experimental results.

2.2. Solid oxide fuel cell

Simulation studies of SOFC using Aspen Plus can be found in literatures [46,47]. The Gibbs reactor was used to simulate the anode in these studies. The Gibbs reactor doesn't require reaction stichometry and kinetics [48]. However, a 0D model is unable to evaluate the operating parameters along the length of the anode. Therefore, to incorporate the MSR and WGS kinetics and to analyze the operating parameter along the length of the anode, a 1D plug flow reactor (PFR) instead of a Gibbs reactor is used. The process flow diagram of the SOFC system is shown in Fig. 1, and anode design parameters are presented in Table 2.

Syngas is fed in at the anode side, while air is presented at the cathode side with an air–fuel stoichiometric ratio (AF) of 1.2:1. The model is divided into 10 sub-cells and validated along the length of the anode. Syngas composition and operating conditions are summarized in Table 3 for the validation of the SOFC model. The TPB is represented with the *RStoic* reactor in the model.

2.2.1. Electrochemical model

The MSR, WGS, and electrochemical reactions coincide in the SOFC, which can be seen in R3, R4, R7 and R8, respectively. The ability to handle half-electrochemical reactions is not inherent to Aspen Plus. Hence, electrochemical reactions (R7 and R8) are combined into a singular chemical reaction (R9). The previous studies showed that the representation of both electrochemical reactions with a single chemical reaction didn't detriment the simulation accuracy because both reactions coincide in the SOFC [46,47,50].

$$H_2 + O^{2-} \rightarrow H_2O + 2e^- \quad (R7)$$

$$0.5O_2 + 2e^- \rightarrow O^{2-} \# \quad (R8)$$

$$CO + O^{2-} \rightarrow CO_2 + 2e^- \quad (R9)$$

Table 1
Rice husk experimental value validation (RMS error 4.58%).

Syngas Composition (mol %)	This model	Reference experimental results for validation [45]
CH_4	0.10	6.22
CO	22.31	22.70
CO_2	22.58	22.20
H_2	55.01	48.88

Table 2
SOFC design parameters for simulation.

Parameter	Value
Anode	Ni/YSZ
Anode thickness (mm)	0.55
Anode porosity (–)	0.3
Anode density (kg/m^3)	7740
RPlug diameter (m)	1.04×10^{-6}
RPlug length (m)	0.0112

Table 3
Syngas composition and operating parameters for validation [49].

Parameter	Value
Temperature (°C)	700
Pressure (bar)	1
SC	1
Flow (L/hour)	3.3
Air/fuel ratio (mole/mole)	1.2
Syngas composition (mole%)	
CH_4	2
H_2	18
H_2O	10
N_2	39
CO	18
CO_2	13

The electrochemical oxidation reactions of H_2 and CO are described by reactions, R7 and R9, respectively. There is a consensus that H_2 is preferentially oxidized at TBP and produces a major fraction of the total current [51]. However, several studies have debated the co-electrochemical oxidation of CO and H_2. For example, Tabish et al. [52] reported that CO contributed only 3% of total current when an equimolar mixture of H_2/CO was used in the presence of Ni anode. It is also evident that the CO oxidation reaction is 2–3 times slower than H_2 oxidation [53]. Thus, CO is preferably involved in the WGS reaction rather than an electrochemical reaction when H_2 and CO are both present in the gas mixture [54–56]. Moreover, Li et al. [57] claimed that CO and H_2 yield the same electromotive force; hence, no distinction is required to model the electrochemical reaction. Therefore, the electrochemical oxidation of CO in this fuel cell model is neglected.

A single cell, fueled with hydrogen, can generate a theoretical Nernst potential of 1.229 V under standard operating conditions (T = 0 °C and P = 1 atm). This theoretical potential can be used to estimate the theoretical reversible open-circuit voltage (OCV) using the following equation:

$$E_{rev}(P,T) = E^o(T,P^o) - \frac{RT}{2F}\ln\left(\frac{P_{H_2O}}{P_{H_2}\sqrt{P_{O_2}}}\right) \quad (1)$$

while

$$E^o(T,P^o) = -\frac{\nabla g^o}{2F} \quad (2)$$

$$\nabla g^o = 0.053T - 245.58 \quad (3)$$

where T (K) is the temperature, P (bar) is the pressure, P_i (bar) represents the partial pressure of ith specie, F (C/mol) denotes the Faraday's constant, and ∇g^o (kJ/mol) is the Gibbs free energy. The voltage across the cell can be derived by:

$$V_{cell} = E_{rev} - U_L - i_{ele}R_{tot} \quad (4)$$

where V_{cell} (V) is cell voltage, i_{ele} (A/m^2) is the current density, R_{tot} (Ω) is total resistance, and U_L represents the loss in potential due to the electrical resistance in the electrolyte and possibly also due to the crossover of gases via microcracks and fissures in the electrolyte while measuring OCV. U_L is generally neglected in the equation because OCV is equivalent to E_{rev} as

$$V_{cell} = E_{rev} - i_{ele} SR_{tot} \tag{5}$$

R_{tot} can be estimated using the empirical relation as shown in the equation

$$R_{tot} = k_{o,ele} \exp\left(\frac{-E_{a,ele}}{RT}\right) \tag{6}$$

where $k_{o,ele}$ is the constant coefficient, and $E_{a,ele}$ is the activation energy. For the known value of V_{cell}, i_{ele} can be calculated using the equation.

$$i_{ele} = \frac{E_{rev} - V_{cell}}{SR_{tot}} \tag{7}$$

2.2.2. Internal reforming model

MSR reaction (R3) and WGS reaction (R4) generate H_2 which is consumed as the fuel in SOFC. The reforming kinetics are critical in SOFC modelling, and it can be affected by different factors such as anode material, partial pressure of fuel and steam, operating temperature, etc. [58] Multiple kinetic expressions are presented in the literature for MSR kinetics [59–62]. The power-law (PL) kinetic model of Achenbach et al. [63] is used for the present study.

$$r_{MSR}\left(\frac{mol}{s\, m^2 bar}\right) = 4274 e^{-\frac{82000}{RT}} P_{CH_4} P_{H_2O}^{-1.25} \tag{8}$$

where P_i is the partial pressure of i^{th} specie, R is the gas constant (8.314 J/mole/K), and T (K) is the operating temperature of SOFC. WGS reaction (R4) is generally considered equilibrium during the modelling studies [64–66]. However, kinetic studies of WGS are available in literatures [67,68]. Therefore, the WGS kinetic model of Xu et al. [69] is used for the present study to avoid overestimating the temperature profile due to the equilibrium WGS reaction.

$$r_{WGS} = \frac{\frac{k_{WGS}}{P_{H_2}}\left(P_{co} P_{H_2O} - \frac{P_{H_2} P_{CO_2}}{K_{WGS}}\right)}{(DEN)^2} \tag{9}$$

where k_{WGS} is the rate constant of WGS reaction which follows the Arrhenius law, K_{WGS} is the equilibrium coefficient of WGS reaction which is the function of temperature, *DEN* is the denominator item with

$$DEN = 1 + K_{CO} P_{CO} + K_{H_2} P_{H_2} + \frac{K_{H_2O} P_{H_2O}}{P_{H_2}} \tag{10}$$

where K_i is the correction factor of component i which varies against temperature.

The rate of the reforming reaction varies along the length of the anode and has the maximum value near the inlet of the anode [70]. Therefore, the reactor model "RPlug" is used in Aspen Plus to represent the SOFC anode. Furthermore, each SOFC cell is divided into ten equal-sized modules to measure the operating variables along the anode length.

2.2.3. Carbon deposition probability

The methane converstion is presented as in Equation (11). The carbon deposition probability is calculated by the ratio of the existing carbon fraction of the syngas and the carbon deposition cutoff line, as shown as Equation (12), where C_{frac} is the existing carbon fraction of the syngas and C_{curoff} is the carbon deposition cutoff line which is determined using Equation (13). When the existing carbon fraction of the syngas is beyond the carbon deposition cutoff line, carbon formation will occur.

$$CH_4 conversion = 1 - \frac{CH_{4,\,out}}{CH_{4,\,in}} \tag{11}$$

$$Carbon\ deposition\ probability = \frac{C_{frac}}{C_{cutoff}} \tag{12}$$

$$C_{cutoff} = \left(-1.0 \times 10^{-3} T + 0.95\right) H_{frac}^2 + \left(4.5 \times 10^{-4} T - 0.87\right) H_{frac} + \left(1.8 \times 10^{-3} T + 0.29\right) \tag{13}$$

where $CH_{4,\,in}$ and $CH_{4,\,out}$ mole flow of CH_4 in SOFC inlet and outlet stream, respectively. The carbon deposition cutoff line is only applicable for temperatures between 400 and 1000 °C with an average error of 10%, where T is the feed (syngas) temperature in °C and H_{frac} and C_{frac} are the mole fraction of hydrogen and carbon in the syngas. Using Eq. (12), carbon deposition is theoretically predicted when the calculated value is larger than 1.

The model is validated against the reported results of Fan et al. [18]. The results presented in Fig. S4a agree with the literature with an acceptable accuracy. All Aspen simulation reported values to lie within the range of the literature values with a deviation of ±5%.

2.3. Integrated gasifier-SOFC system

Validated models of gasifier and SOFC combined to create an integrated gasifier SOFC system. Coal, marine algae, and sugarcane bagasse are used as feeds with their proximate and ultimate analysis listed in Table 4. These are selected to compare the current commonly used coal with the potential biomass alternatives, which are marine algae and sugarcane bagasse, in the application of the gasifier-SOFC system.

The power density and total efficiency are the major performance indicators of the gasifier-SOFC system. The highest value of power density shows the optimum power production. The efficiency of integrated gasifier-SOFC ($\eta_{overall}$) is estimated using the electrical and thermal efficiency of the system and can be represented as:

$$\eta_{overall} = \left[\frac{P_{SOFC} + Q}{\dot{m}_{biomass}\, x\, LHV_{biomass}}\right] \tag{14}$$

where P_{SOFC} (kW) is the power generated by SOFC, $\dot{m}_{biomass}$ (kg/s) is biomass mass flow rate, $LHV_{biomass}$ (kJ/kg) is the lower heating value of the biomass, and Q (kW) is the energy generated in the process.

2.4. Heat integration

The exhaust stream of SOFC contains unutilized fuel, which can be used for heat integration after the combustion. The energy requirement for the whole process is listed as follows:

Table 4
Feeds selected for manipulated variables.

Variables (wt%)	Coal	Marine algae	Sugarcane bagasse
Proximate analysis			
Volatile	30.8	45.1	80.5
Moisture	5.5	10.7	5.0
Fixed Carbon	43.9	23.1	10.5
Ash	19.8	21.1	4.0
Ultimate analysis			
C	78.2	43.2	42.3
H	5.2	6.2	6.1
O	13.6	45.8	46.4
N	1.3	2.2	1.2
S	1.7	2.6	–

i. Steam generation for gasification;
ii. Syngas heating;
iii. SOFC air pre-heating;
iv. Heat requirement of gasifier;
v. Biomass dryer air pre-heating.

The energy requirement of the process can be fulfilled with the energy of the exhaust stream, as shown in Fig. 1. The exhaust gases, after combustion, first generate steam for gasification in the boiler (E-3). Secondly, syngas and air were pre-heated up to the operating temperature of SOFC in E-1 and E-2, respectively. Finally, the air for the dryer is pre-heated to heat the biomass to the temperature of 70 °C in E-5. The residue heat of the flue gas is further used to generate high-pressure (HP) steam for power generation in the steam turbine. The HP steam is generated in E-4 and passes through a turbine to generate electricity. Partially condensed steam further cools down in E-6 by cooling water and pumped back into the boiler. The details of Aspen Plus simulation and heat integration for the representative case of coal at 900 °C syngas temperature are summarized in **Supplement**.

3. Sensitivity study and process optimization

3.1. Sensitivity analysis

The optimal operating conditions for the integrated gasifier-SOFC system were determined by evaluating the process performance under various gasifier temperatures, external steam-to-carbon ratio (SC_e), steam-to-biomass ratio (SB), current density and SOFC feed temperature. Then based on the sensitivity analysis, an optimization study was carried out for each feedstock to get the maximum power output. These modelling conditions applied a 1577 kg/h of the feed rate, SB of 1, 750 °C of gasifier temperature, SC_e of 1.0, voltage of 0.8 V, and 700 °C of

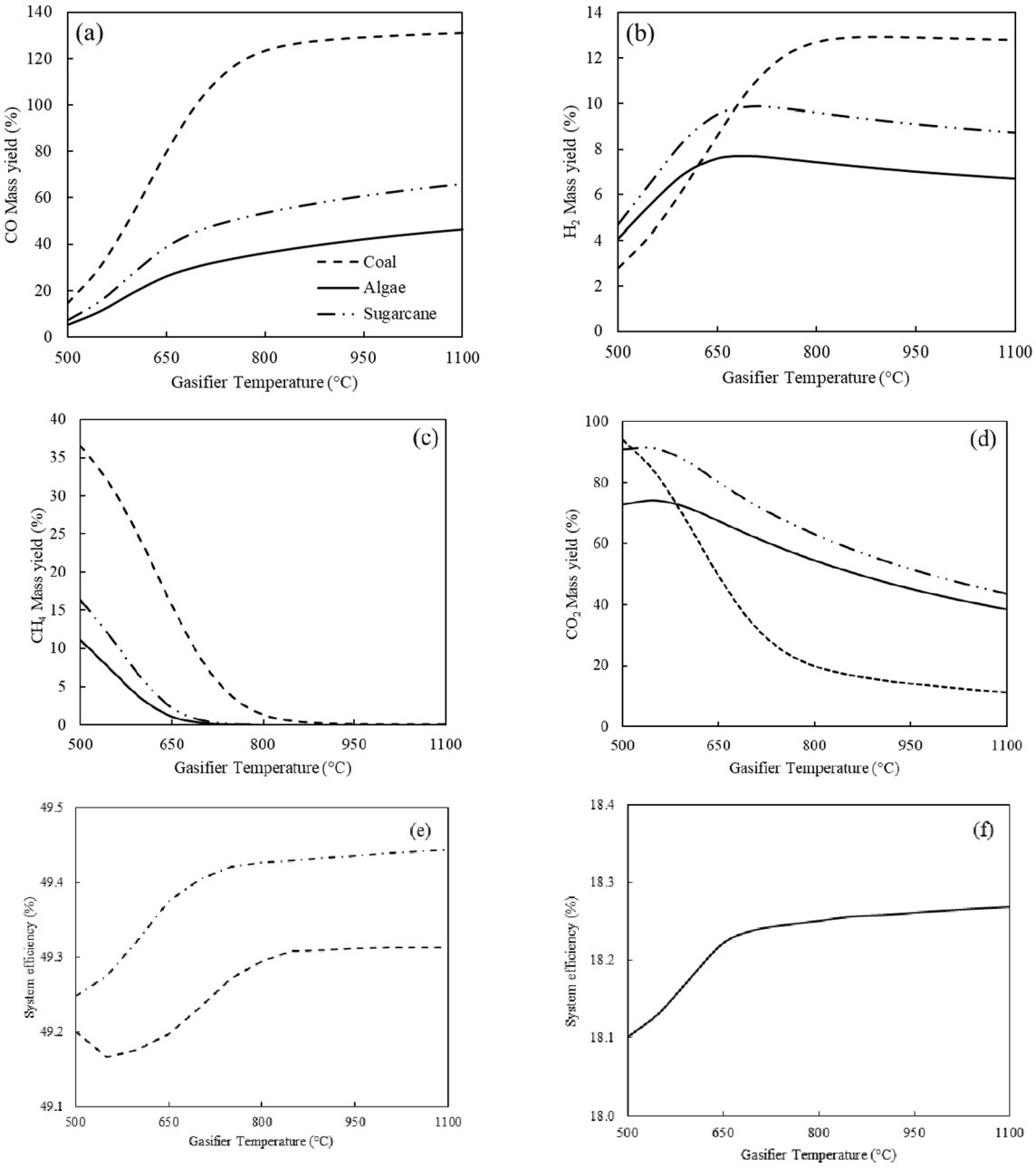

Fig. 2. Effect of gasifier temperature on syngas for coal, marine algae, and sugarcane bagasse at $SC_e = 1.0$, SB = 1.0 and feed flow rate = 1577 kg/h on (a) CO yield, (b) H_2 yield, (c) CH_4 yield, (d) CO_2 yield, and (e) and (f) system efficiency.

the feed temperature unless specified on the plots.

3.1.1. Effects of gasifier temperature on syngas yield

The effect of gasifier temperature on syngas component yields and system efficiency is shown in Fig. 2. The yield of CH_4 (Fig. 2**c**) decreases with the increase in the gasifier temperature mainly due to the conversion of CH_4 in H_2 and CO via MSR reaction (R3) at higher temperatures. Coal gives the highest CH_4 yield of 36.6% at 500 °C, followed by sugarcane bagasse and algae with 16.4 and 11.8%, respectively. On the other hand, CO yield (Fig. 2**a**) increases with the increase in gasifier temperature throughout the considered temperature range (500–1000 °C). The increase in CO yield is sharp at lower temperatures (500–800 °C) for all feedstocks, mainly due to the high reaction rate of the steam reforming reaction, which is also seen by the slight increase of CO_2 yield in Fig. 2**d** attributed to the WGS reaction. At 800–1100 °C, the increase in CO yield is relatively steady due to the decrease in WGS rate at higher temperatures. Coal gives the highest CO yield at all temperatures due to the oxidation of carbon in the presence of H_2O to produce CO and H_2, as shown in R2. After coal, sugarcane bagasse has a higher CO yield than marine algae. It is noted that at occurrent cases the yield of CO is beyond 100%. It is because the yields are calculated based on the mass of coal or biomass without considering the addition of steam. The carbon mass balances for all experiments keep at 100%, which was approved by the calculation using an experiment as an example in

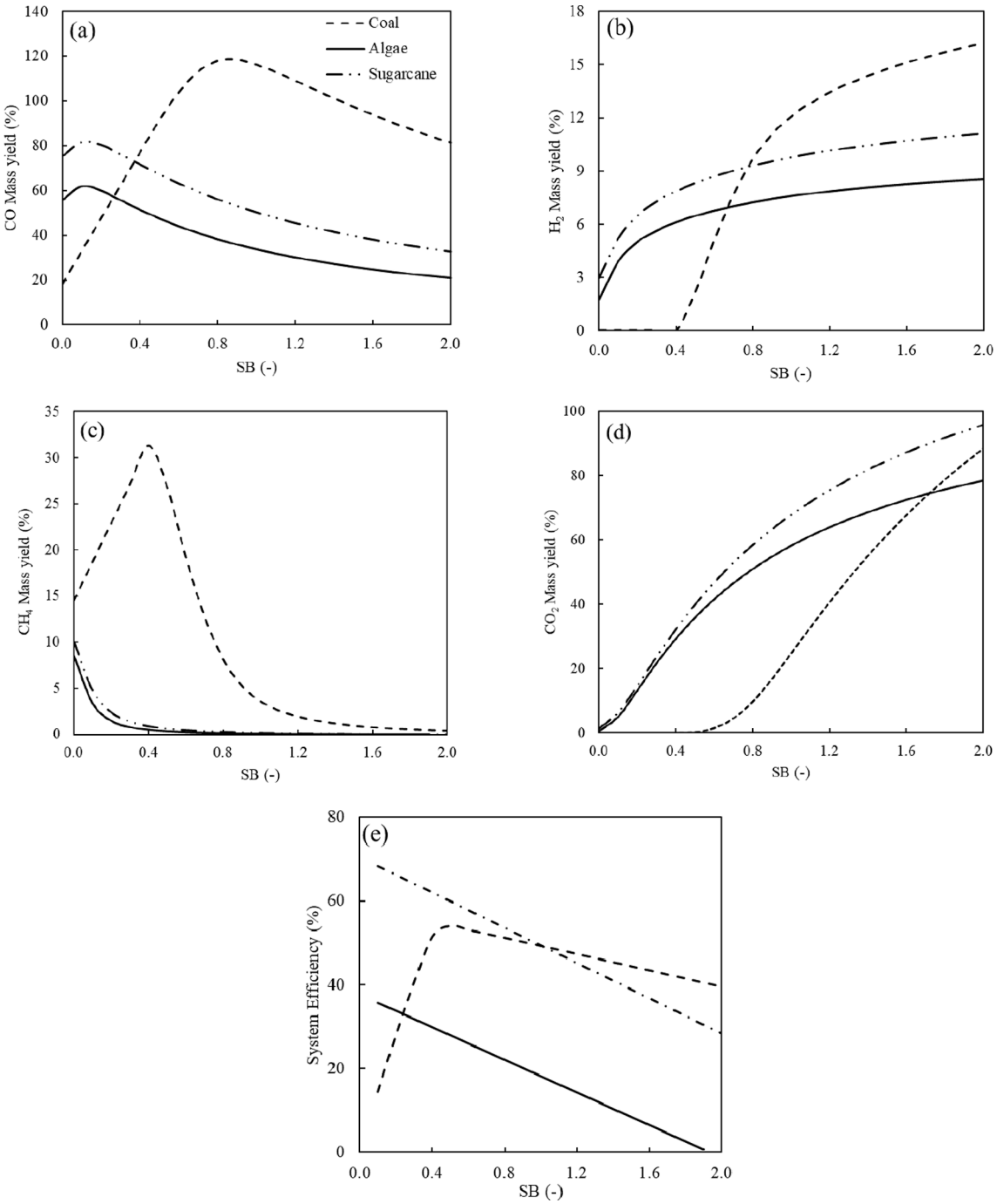

Fig. 3. Effect of steam to biomass ratio on syngas for Coal, Marine algae, and Sugarcane bagasse at gasifier temperature = 750 °C and feed flow rate = 1577 kg/h on (a) CO yield, (b) H_2 yield, (c) CH_4 yield, (d) CO_2 yield, and (e) system efficiency.

Supplement.

H_2 yield (Fig. 2**b**), on the other hand, increases with the increase in temperature at the low-temperature range and then starts to decrease with a further increase in the gasifier temperature. Maximum H_2 yield for coal, marine algae, and sugarcane bagasse is 12.9, 8.2, and 9.8 % at the operating temperature of 900, 700, and 700 °C, respectively.

Fig. 2**e and f** show the effects of gasifier temperature on the system efficiencies for coal and sugarcane bagasse, and for algae, respectively. Among the considered operating parameters, gasifier temperature has minimum effect on the system efficiency than other operating parameters. The maximum increase of 1% in system efficiency was recorded for Algae when the gasifier temperature increased from 500 to 1100 °C. Coal and sugarcane bagasse has the increase of 0.3 and 0.4%, respectively.

3.1.2. *Effects of steam-to-biomass ratio (SB) on syngas yield*

Fig. 3**a–d** show the effect of SB on the syngas component yield. CO yield increases with the increase in SB at a low value (<1) and then decreases (Fig. 3**a**). Maximum CO yield for coal, marine algae, and sugarcane bagasse is 118.3, 65.5, and 80.9 % at the SB of 0.9, 0.1, and 0.1, respectively. After the maximum value, CO yield starts to decrease mainly due to the increase in steam partial pressure, which eventually causes more conversion of CO into CO_2 via WGS (R4), which can also be proved by the increasing of the yield of CO_2 at higher SB ratio as shown in Fig. 3**d**.

H_2 yield increases with SB throughout the considered temperature range (0–2) (Fig. 3**b**). Coal gives the highest H_2 yield at the highest SB because CO converts to CO_2 and H_2 at higher SB values.

Unlike the other two biomasses, coal gives a different CH_4 yield trend (Fig. 3**c**). CH_4 yield increases from 14.5% and reaches the maximum value of 31.3% at the SB of 0.4, then decreases until it approaches zero. This might result from the competition of methanation and steam reforming. Coal contains the higher carbon content than the other two feedstocks. At lower SB, the methanation which enhances the CH_4 yield may dominate the reaction and the rate of MSR remains low due to the low steam partial pressure; therefore, CH_4 yield increases for coal at lower SB.

For coal, system efficiency increases sharply with the increase in SB till the value of 0.5 and then decreases steadily. Hydrogen yield is very low at SB < 0.5, which results in lower power density, as shown in Fig. 3**e**. Therefore, system efficiency remained low for SB < 0.5. SB negatively affect the system efficiency throughout the considered operating range (0–2) for marine algae and sugarcane bagasse. Coal has a maximum efficiency of 54.1% at SB = 0.5 while marine algae and sugarcane bagasse has the maximum system efficiency of 35.7 and 68.3% when SB is negligible.

It is noted that the system efficiency mentioned in this paper refers the energy efficiency only. It is assumed that 100% of the syngas produced in gasification flows to fuel cell with ignorable carbon formation.

3.1.3. *Effect of SOFC feed temperature*

Fig. 4**a-d** show the effect of SOFC feed temperature on power density, carbon deposition, and the system efficiencies for coal, sugarcane bagasse, and algae, respectively. The power density (Fig. 4**a**) increases with the increase in the SOFC feed temperature at a constant voltage of 0.8 V. This is because of the increased cell voltage associated with the Nernst Equation at higher temperatures. A similar power density trend can also be found in the literature [71]. However, there is a slight difference between all feedstocks' power densities under consideration. Although high-temperature results in high power density, it also leads to thermal stresses in the anode. Therefore, SOFC temperature should be operated at an intermediate temperature range (500–800 °C) [72].

The chance for carbon deposition occurs throughout the considered temperature range for feedstocks is negligible, as shown in Fig. 4**b**.

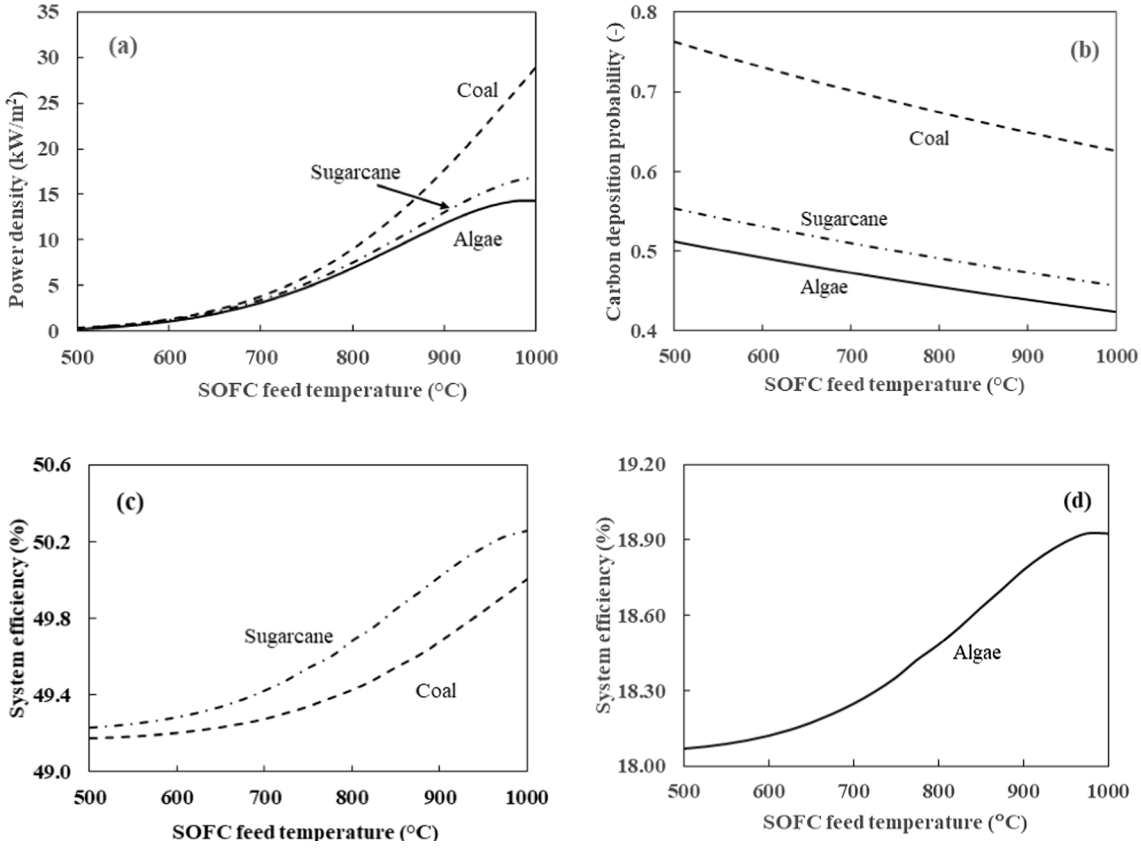

Fig. 4. Effect of SOFC feed temperature at SC_e = 1.0, SB = 1.0, and gasifier temperature of 750 °C on (a) power density, (b) carbon deposition probability, and (c) and (d) system efficiencies for coal, sugarcane bagasse, and algae, respectively.

However, coal is more susceptible to carbon formation than the biomasses throughout the considered temperature range (500–1000 °C) as its C_{cutoff} (the carbon formation cutoff line) is lower than the biomasses. The C_{cutoff} increases with the rise of SOFC feed temperature. The decrease in carbon deposition probability within the considered temperature range (500–1000 °C) is estimated at 18.0, 17.0, and 17.5 for coal, marine algae, and sugarcane bagasse, respectively. Therefore, to avoid carbon formation at lower SC_e (which will be discussed more in Section 3.1.5), SOFC needs to be operated at a higher temperature for coal than the biomass feedstocks.

Like gasifier temperature, SOFC feed temperature has little effect on the overall efficiency (Fig. 4**c** and **d**). The maximum increase of 4.7 % in system efficiency was recorded for algae when SOFC feed temperature increased from 500 to 1000 °C. Coal and sugarcane bagasse have the increases of 1.6% and 2.1%, respectively.

3.1.4. *Effect of the current density*

Fig. 5**a** and **b** show the trends of the open circuit voltage and power density with respect to the current density for coal, marine algae, and sugarcane bagasse, respectively. The open circuit voltage (Fig. 5**a**) and power density (Fig. 5**b**) of sugarcane bagasse are slightly higher than coal and marine algae when the cell current density is more than 10,000 A/m^2. However, when the cell current density is lower than that value, both voltage and power density of coal become the highest. The maximum power density of marine algae, coal, and sugarcane bagasse are calculated as 5.53, 6.08, and 6.22 kW/m^2, respectively, when the voltage is at 0.5 V and the current density approaches 12,000 A/m^2. Power density starts to drop beyond this point.

3.1.5. *Effect of external steam-to-carbon ratio (SC_e)*

Fig. 6**a and b** show the effect of SC_e on SOFC power density and carbon deposition probability, respectively. Coal shows a different power density trend than marine algae and sugarcane bagasse (Fig. 6**a**). It has a maximum drop of 63.8% in power density with respect to the maximum power density. The power density firstly increases with the increase in the SC_e, then decreases steadily after achieving the maximum value of 3.82 kW/m^2 at $SC_e = 1.0$. Marine algae and sugarcane bagasse have a power density drop of 63.0 and 62.4%, respectively. The power density for those biomass feedstocks gradually decreases with the increase in the SC_e because high water content causes fuel dilution, which reduces SOFC power density. Although lower SC_e results in higher power density but is more suspectable to carbon deposition. However, in the presented operating conditions, the carbon deposition is negligible and only coal can cause carbon deposition at SC_e of 0.1. After this, no theoretical carbon was observed for all feedstocks, as shown in Fig. 6**b**.

SC_e effect on system efficiency follows the same trend as SB but with different magnitudes (Fig. 6**c**). For coal, system efficiency increases sharply at the beginning with the increase in SC till the value of 0.3 and then decreases steadily. SC_e negatively affect the system efficiency throughout the considered operating range (0–2) for marine algae and sugarcane bagasse. Maximum overall efficiency is achieved when no external steam is added to the system. At the same time, coal has a maximum efficiency of 55.7% at $SC_e = 0.3$. Higher SC causes the dilution of syngas, reducing the power output of SOFC.

Fig. 6**d** shows the variation of actual steam-to-carbon ratio (SC_a) in SOFC feed with the change in the SC_e. SC_a is inherent to the moisture content of the syngas after gasification. Marine algae have the highest moisture content in the syngas; therefore, the minimum SC_a for marine algae is estimated as 1.20 when no external steam is introduced. Unlike marine algae, sugarcane bagasse and coal have $SC_a < 1.0$ at low SC_e. $SC_a = 1.0$ is achieved when SC_e crosses the value of 0.1 and 1.3 for sugarcane bagasse and coal, respectively. As maximum power density is achieved when SCa approaches the unity value, low SC_a of coal caused the opposite power density trend in Fig. 6**a**.

As lower SC_a favours the power density, as shown in Fig. 6**a** and **b**, it may expect that the change in gasification temperature may decrease the SC_a up to the no carbon deposition zone.

3.2. *Optimization for maximum power density and hydrogen yield*

The maximum power density for the integrated gasifier-SOFC system is evaluated by optimizing the independent variables (voltage, SB, and SC_e) and dependent variables (power density). In addition, constraints to avoid carbon deposition for an iterative process are followed. The gasification temperature is not included in the optimization study without effect on the system efficiency despite increased power density. The optimization study was carried out at two different syngas temperatures, and the results are summarized in Table 5.

According to the study, a high SB ratio in the gasifier negatively affects the power density of SOFC. Coal has the highest SB ratio; hence, it has the lowest power density of 6.79 and 38.74 kW/m^2 under the optimized conditions. The rise in syngas temperature elevates the power density, but the relative difference between the power density of different feedstock remains the same.

The steam requirement in the gasifier is directly related to the carbon content of the feedstock. In this study, all feedstocks have different carbon percentages in the ultimate analysis. Therefore, the steam requirement in the gasifier varies significantly when each case is optimized. Coal requires the highest steam for gasification because it contains 78.2 % carbon. SB of coal is 1.29 and 1.27 at 700 and 900 °C, respectively. Marine algae require the lowest steam due to the lowest carbon content than the other feedstocks.

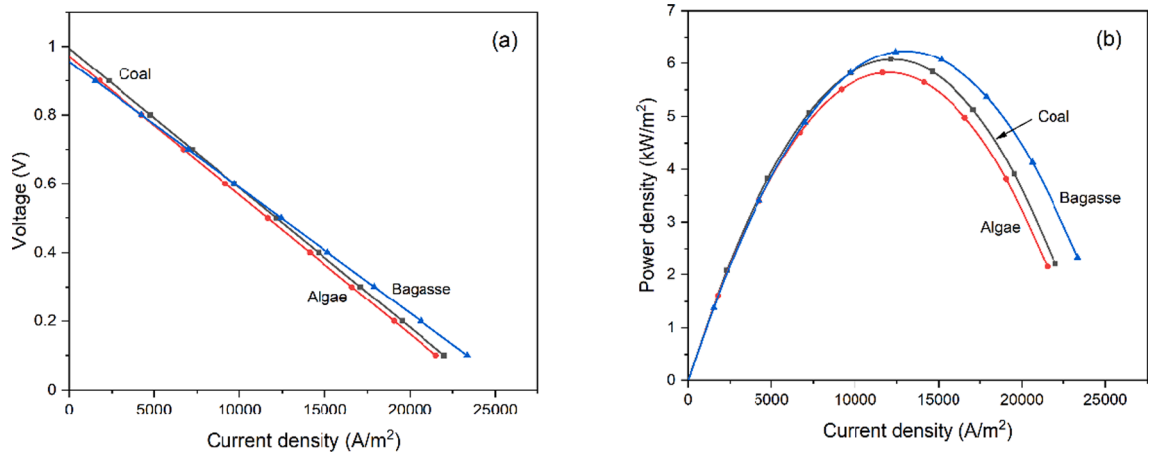

Fig. 5. Open circuit voltages (a) and power densities (b) profiles versus the current densities of coal, marine algae, and sugarcane bagasse at $SC_e = 1$, SOFC feed temperature = 700 °C, gasifier temperature = 750 °C, and SB = 1.

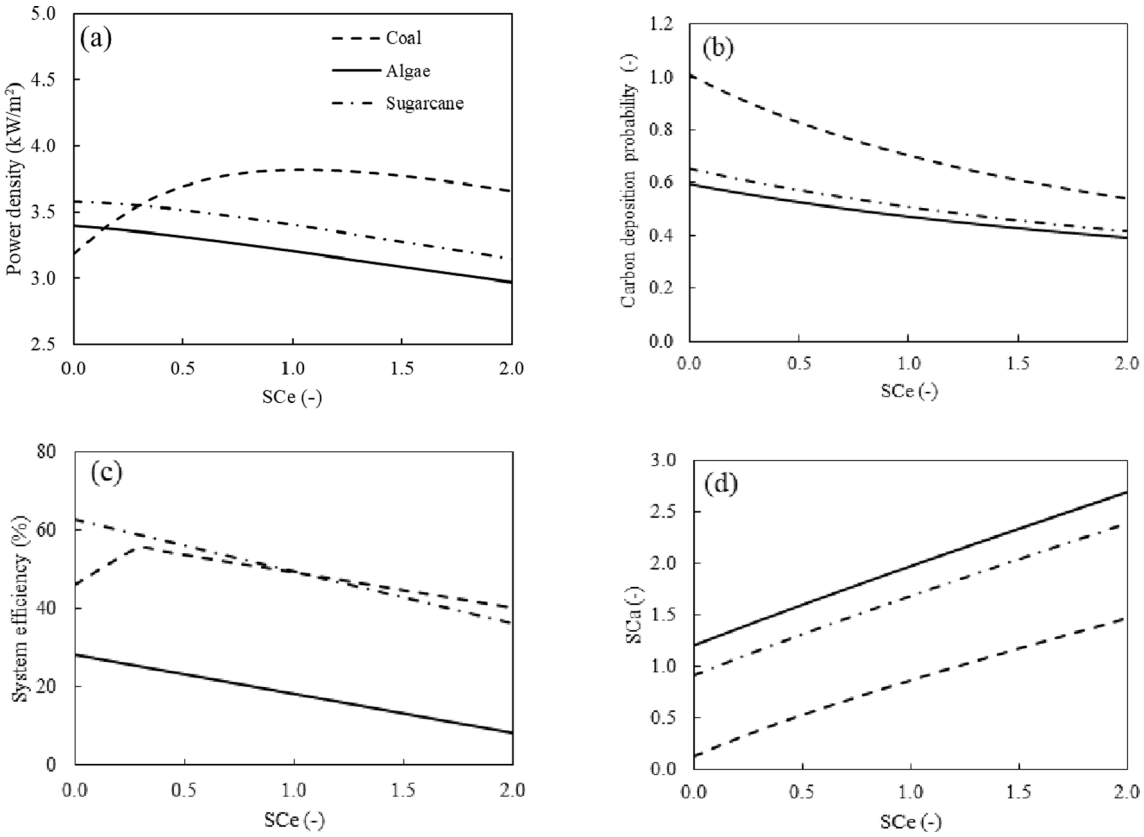

Fig. 6. Effect of external steam to carbon ratio at SOFC feed temperature = 700 °C, gasifier temperature = 750 °C, SB = 1.0, and feed flow rate = 1577 kg/h on (a) power density, (b) carbon deposition probability, (c) system efficiency, and (d) actual steam to carbon ratio.

Table 5
Optimisation Result with maximised power density.

Results	Coal	Marine Algae	Sugarcane Bagasse	Coal	Marine Algae	Sugarcane Bagasse
SOFC Inlet Temperature (°C)	700			900		
Power Density (kW/m^2)	6.79	7.04	7.02	38.74	39.44	39.33
Syngas Composition (mol %)						
CH_4	0.72	0.87	0.85	0.75	0.86	0.92
H_2	51.73	47.81	48.31	51.81	47.81	48.32
CO	28.20	34.14	33.33	28.62	33.87	34.10
Voltage (V)	0.49	0.48	0.48	0.46	0.45	0.45
SB Ratio (mass/mass)	1.29	0.30	0.36	1.27	0.30	0.34
C/O Ratio (mass/mass)	0.71	0.38	0.46	0.71	0.38	0.46
Gasifier Temperature °C	750	750	750	750	750	750
SC_e (mol/mol)	1.77	1.72	1.66	1.53	1.59	1.59
SC_a (mol/mol)	2.05	1.93	1.88	1.82	1.76	1.79
Total Estimated Power (kW)	25.81	26.77	26.66	147.21	149.87	149.47
System Efficiency (%)	39.40	26.47	54.26	42.73	28.52	57.62

The total steam requirement depends on the syngas composition. Algae and sugarcane bagasse have almost the same syngas composition and, therefore, SC_a. Unlike biomass feedstocks, coal has the lowest CH_4 content in the syngas, requiring less SC_a. The chance of carbon deposition for the optimum conditions found by Aspen Plus is calculated using Eq. (5). They all lie outside the carbon deposition region, so no carbon deposition occurs theoretically. As a result, it is safe to run in those operational conditions.

It can be seen the increase in SOFC feed temperature increases the power density and overall system efficiency. Additionally, optimized steam requirement decreases with the increase in SOFC feed temperature. So, it can be stated that the process moves away from carbon deposition at lower SC_a if the system is optimized at higher SOFC feed temperatures.

Marine algae have the highest power density under optimized conditions. However, the overall efficiency of marine algae remains low due to the low energy density of the feedstock. So, based on the combined electrical and thermal efficiency of the system, sugarcane bagasse proved to be the most efficient among the considered feedstocks.

4. Conclusion

Using steam as the agent, the combined gasifier-SOFC system converts feedstock to syngas which goes through the water separation to dry syngas. Then, it flows to the SOFC to co-produce power and H_2. The novel 0D integrated gasifier-SOFC model was developed in Aspen Plus

for the hydrogen and power generation using coal, marine algae, and sugarcane bagasse. The model gasifier and SOFC models were individually validated against experimental results found in the literature. To compare all the feedstocks in terms of power density, gasifier temperature, SOFC feed temperature, CH_4, H_2, and CO yield, the gasifier temperature of 750 °C, the pressure of 1.01 bar, SB of 1.0 and SC_e of 1.0 were taken. After the sensitivity analysis, the optimization study was carried out at SOFC feed temperatures of 700 °C and 900 °C. The outcomes of the optimization study are listed:

- A low SB ratio in the gasifier gives the high-power density of SOFC. As a result, marine algae has the highest power density of 7.04 and 39.44 kW/m^2 under the gasifier temperatures of 700 and 900 °C, respectively.
- An increase in the syngas temperature improves the power density and system efficiency.
- Feedstock with higher carbon content requires high SB for complete gasification. Coal contains 78.2% fixed carbon, therefore, the steam requirement for gasification is highest for coal.
- Feedstock with high ash and moisture content has a lower overall efficiency than high energy content feedstocks such as sugarcane bagasse.

Considering the optimization results, biomasses with high ash content may be more challenging to run than coal because of the low efficiency and the requirement of ash removal. However, this gasifier-SOFC model did not consider the effect of impurities such as sulfur which limit the accuracy and comprehensiveness of the simulation.

CRediT authorship contribution statement

Ben Britt: Software, Methodology, Investigation, Formal analysis, Data curation, Conceptualization, Writing - original draft. **Mateus Rocha:** Writing - review & editing. **Shou-Han Zhou:** Writing - review & editing. **Weiwei Cai:** Writing - review & editing.

Declaration of Competing Interest

The authors declare that they have no known competing financial interests or personal relationships that could have appeared to influence the work reported in this paper.

Data availability

No data was used for the research described in the article.

Acknowledgment

The authors would like to thank James Cook University for providing the Australian PhD scholarship and financial support, and Ms Beatrix Nessia Kamadjaja for joining the paper discussion at the early stage.

Appendix A. Supplementary material

Supplementary data to this article can be found online at https://doi.org/10.1016/j.fuel.2023.129529.

References

[1] Musharavati F, et al. Multi-objective optimization of a biomass gasification to generate electricity and desalinated water using Grey Wolf Optimizer and artificial neural network. Chemosphere 2022;287:131980.
[2] Bui M, et al. Delivering carbon negative electricity, heat and hydrogen with BECCS – comparing the options. Int J Hydrogen Energy 2021;46(29):15298–321.
[3] Dincer I, Acar C. Review and evaluation of hydrogen production methods for better sustainability. Int J Hydrogen Energy 2015;40(34):11094–111.
[4] Binder M, et al. Hydrogen from biomass gasification. IEA Bioenergy; 2018.
[5] Middelhoff E, et al. Hybrid concentrated solar biomass (HCSB) plant for electricity generation in Australia: design and evaluation of techno-economic and environmental performance. Energ Conver Manage 2021;240:114244.
[6] Nandimandalam H, Gude VG, Marufuzzaman M. Environmental impact assessment of biomass supported electricity generation for sustainable rural energy systems-a case study of Grenada County, Mississippi, USA. Sci Total Environ 2022;802:149716.
[7] Manna J, et al. Opportunities for green hydrogen production in petroleum refining and ammonia synthesis industries in India. Int J Hydrogen Energy 2021;46(77):38212–31.
[8] Nami H, et al. Techno-economic analysis of current and emerging electrolysis technologies for green hydrogen production. Energ Conver Manage 2022;269:116162.
[9] Marcoberardino GD, et al. Green hydrogen production from raw biogas: a techno-economic investigation of conventional processes using pressure swing adsorption unit. Processes 2018;6(3):19.
[10] Ma C, et al. Numerical study on solar spouted bed reactor for conversion of biomass into hydrogen-rich gas by steam gasification. Int J Hydrogen Energy 2020;45(58):33136–50.
[11] Lu X, et al. Gasification of coal and biomass as a net carbon-negative power source for environment-friendly electricity generation in China. In: Proceedings of the national academy of sciences 2019; 116(17): 8206–13.
[12] Parthasarathy P, Narayanan KS. Hydrogen production from steam gasification of biomass: Influence of process parameters on hydrogen yield – a review. Renew Energy 2014;66:570–9.
[13] Singh AP, et al. Steam reforming of methane and methanol in simulated macro & micro-scale membrane reactors: selective separation of hydrogen for optimum conversion. J Nat Gas Sci Eng 2014;18:286–95.
[14] Molino A, et al. Biofuels production by biomass gasification: a review. Energies 2018;11(4):811.
[15] Minette F, et al. Intrinsic kinetics of steam methane reforming on a thin, nanostructured and adherent Ni coating. Appl Catal B 2018;238:184–97.
[16] Iwahara H, et al. Ca1-xCexMnO3±δ as new air electrode material for SOFC. Denki Kagaku 1989;57(6):591–4.
[17] Chen L, et al. Catalytic hydrogen production from methane: a review on recent progress and prospect. Catalysts 2020;10(8):858.
[18] Fan L, et al. Computational studies for the evaluation of fuel flexibility in solid oxide fuel cells: a case with biosyngas. Fuel Cells 2013;13(3):410–27.
[19] Gür TM. Comprehensive review of methane conversion in solid oxide fuel cells: prospects for efficient electricity generation from natural gas. Prog Energy Combust Sci 2016;54:1–64.
[20] Marcantonio V, et al. Main issues of the impact of tar, H2S, HCl and alkali metal from biomass-gasification derived syngas on the SOFC anode and the related gas cleaning technologies for feeding a SOFC system: a review. Int J Hydrogen Energy 2022;47(1):517–39.
[21] Mermelstein J, Millan M, Brandon NP. The impact of carbon formation on Ni-YSZ anodes from biomass gasification model tars operating in dry conditions. Chem Eng Sci 2009;64(3):492–500.
[22] Baldinelli A, et al. Biomass integrated gasifier-fuel cells: experimental investigation on wood syngas tars impact on NiYSZ-anode solid oxide fuel cells. Energ Conver Manage 2016;128:361–70.
[23] Lorente E, Millan M, Brandon NP. Use of gasification syngas in SOFC: Impact of real tar on anode materials. Int J Hydrogen Energy 2012;37(8):7271–8.
[24] Namioka T, et al. A tolerance criterion for tar concentration in a model wood gas for a nickel/scandia-stabilized zirconia cermet anode in a solid oxide fuel cell. Int J Hydrogen Energy 2012;37(22):17245–52.
[25] Geis M, et al. Coupling SOFCs to biomass gasification – the influence of phenol on cell degradation in simulated bio-syngas. Part I: Electrochemical analysis. Int J Hydrogen Energy 2018;43(45):20417–27.
[26] Mermelstein J, Millan M, Brandon N. The impact of steam and current density on carbon formation from biomass gasification tar on Ni/YSZ, and Ni/CGO solid oxide fuel cell anodes. J Power Sources 2010;195(6):1657–66.
[27] Noichi H, Uddin A, Sasaoka E. Steam reforming of naphthalene as model biomass tar over iron–aluminum and iron–zirconium oxide catalyst catalysts. Fuel Process Technol 2010;91(11):1609–16.
[28] Nilsson S, et al. Gasification of biomass and waste in a staged fluidized bed gasifier: modeling and comparison with one-stage units. Fuel 2012;97:730–40.
[29] Sasaki K, et al. H2S poisoning of solid oxide fuel cells. J Electrochem Soc 2006;153(11):A2023.
[30] Matsuzaki Y, Yasuda I. The poisoning effect of sulfur-containing impurity gas on a SOFC anode: Part I. Dependence on temperature, time, and impurity concentration. Solid State Ion 2000;132(3–4):261–9.
[31] Kupecki J, et al. Numerical model of planar anode supported solid oxide fuel cell fed with fuel containing H2S operated in direct internal reforming mode (DIR-SOFC). Appl Energy 2018;230:1573–84.
[32] Aguilar L, et al. A solid oxide fuel cell operating on hydrogen sulfide (H2S) and sulfur-containing fuels. J Power Sources 2004;135(1):17–24.
[33] Roushanafshar M, et al. Effect of hydrogen sulfide inclusion in syngas feed on the electrocatalytic activity of LST-YDC composite anodes for high temperature SOFC applications. Int J Hydrogen Energy 2012;37(9):7762–70.
[34] Husmann M, et al. Comparison of dolomite and lime as sorbents for in-situ H2S removal with respect to gasification parameters in biomass gasification. Fuel 2016;181:131–8.
[35] Papurello D, Lanzini A. SOFC single cells fed by biogas: experimental tests with trace contaminants. Waste Manag 2018;72:306–12.

[36] Krishnan GN, et al. Development of disposable sorbents for chloride removal from high-temperature coal-derived gases. In: Advanced coal-fired power systems '96 review meeting. West Virginia: Morgantown; 1996. p. 1–11.
[37] Restrepo SYG, et al. Design and operation of a gas cleaning system for biomass gasification in a two-stage air-blown downdraft gasifier to meet quality requirements of solid oxide fuel cells. Biomass Convers Biorefin 2021.
[38] Mutlu ÖÇ, Zeng T. Challenges and opportunities of modeling biomass gasification in aspen plus: a review. Chem Eng Technol 2020;43(9):1674–89.
[39] Kancherla R, et al. Modeling and simulation for design and analysis of membrane-based separation processes. Comput Chem Eng 2021;148:107258.
[40] Ahmed K, Föger K. Analysis of equilibrium and kinetic models of internal reforming on solid oxide fuel cell anodes: effect on voltage, current and temperature distribution. J Power Sources 2017;343:83–93.
[41] Marcantonio V, et al. Biomass steam gasification, high-temperature gas cleaning, and SOFC model: a parametric analysis. Energies 2020;13(22):5936.
[42] Doherty W, Reynolds A, Kennedy D. Aspen plus simulation of biomass gasification in a steam blown dual fluidised bed. In: Materials and processes for energy: communicating current research and technological developments, A. Méndez-Vilas, Editor. 2013, Formatex Research Centre. p. 212–20.
[43] Sreejith CC, Muraleedharan C, Arun PS. Performance prediction of steam gasification of wood using an ASPEN PLUS thermodynamic equilibrium model. Int J Sustain Energ 2014;33:416–34.
[44] Subotić V, et al. Applicability of the SOFC technology for coupling with biomass-gasifier systems: short- and long-term experimental study on SOFC performance and degradation behaviour. Appl Energy 2019;256:113904.
[45] Karmakar MK, Datta AB. Generation of hydrogen rich gas through fluidized bed gasification of biomass. Bioresour Technol 2011;102(2):1907–13.
[46] Zhang W, et al. Simulation of a tubular solid oxide fuel cell stack using AspenPlusTM unit operation models. Energ Conver Manage 2005;46(2):181–96.
[47] Hauck M, Herrmann S, Spliethoff H. Simulation of a reversible SOFC with Aspen Plus. Int J Hydrogen Energy 2017;42(15):10329–40.
[48] Sezer S, Kartal F, Özveren U. Artificial Intelligence Approach in Gasification Integrated Solid Oxide Fuel Cell Cycle. Fuel 2022;311:122591.
[49] Van Biert L, et al. Dynamic modelling of a direct internal reforming solid oxide fuel cell stack based on single cell experiments. Appl Energy 2019;250:976–90.
[50] Ameri M, Mohammadi R. Simulation of an atmospheric SOFC and gas turbine hybrid system using Aspen Plus software. Int J Energy Res 2013;37(5):412–25.
[51] Patel HC, Tabish AN, Aravind PV. Modelling of elementary kinetics of H2 and CO oxidation on ceria pattern cells. Electrochim Acta 2015;182:202–11.
[52] Tabish AN, Patel HC, Aravind PV. Electrochemical oxidation of syngas on nickel and ceria anodes. Electrochim Acta 2017;228:575–85.
[53] Matsuzaki Y, Yasuda I. Electrochemical oxidation of H2 and CO in a H2–H2O - CO - CO2 system at the interface of a Ni-YSZ cermet electrode and YSZ electrolyte. J Electrochem Soc 2000;147(5):1630.
[54] Khaleel MA, et al. A finite element analysis modeling tool for solid oxide fuel cell development: coupled electrochemistry, thermal and flow analysis in MARC®. J Power Sources 2004;130(1):136–48.
[55] Holtappels P, et al. Reaction of CO/CO2 gas mixtures on Ni–YSZ cermet electrodes. J Appl Electrochem 1999;29(5):561–8.
[56] Patel HC, et al. Oxidation of H2, CO and syngas mixtures on ceria and nickel pattern anodes. Appl Energy 2015;154:912–20.
[57] Li P-W, Chyu MK. Simulation of the chemical/electrochemical reactions and heat/mass transfer for a tubular SOFC in a stack. J Power Sources 2003;124(2):487–98.
[58] Faheem HH, et al. A review on mathematical modelling of direct internal reforming- solid oxide fuel cells. J Power Sources 2022;520:230857.
[59] Timmermann H, et al. Kinetics of (reversible) internal reforming of methane in solid oxide fuel cells under stationary and apu conditions. J Power Sources 2010;195(1):214–22.
[60] Ahmed K, Foger K. Kinetics of internal steam reforming of methane on Ni/YSZ-based anodes for solid oxide fuel cells. Catal Today 2000;63(2–4):479–87.
[61] Dicks AL, Pointon KD, Siddle A. Intrinsic reaction kinetics of methane steam reforming on a nickel/zirconia anode. J Power Sources 2000;86(1–2):523–30.
[62] Bebelis S, et al. Intrinsic kinetics of the internal steam reforming of CH4 over a Ni-YSZ-cermet catalyst-electrode. Ind Eng Chem Res 2000;39(12):4920–7.
[63] Achenbach E, Riensche E. Methane/steam reforming kinetics for solid oxide fuel cells. J Power Sources 1994;52(2):283–8.
[64] Wongchanapai S, et al. Selection of suitable operating conditions for planar anode-supported direct-internal-reforming solid-oxide fuel cell. J Power Sources 2012;204:14–24.
[65] Brus G. Experimental and numerical studies on chemically reacting gas flow in the porous structure of a solid oxide fuel cells internal fuel reformer. Int J Hydrogen Energy 2012;37(22):17225–34.
[66] Chalusiak M, et al. A numerical analysis of unsteady transport phenomena in a direct internal reforming solid oxide fuel cell. Int J Heat Mass Transf 2019;131:1032–51.
[67] Durán FJ, Dorado F, Sanchez-Silva L. Exergetic and economic improvement for a steam methane-reforming industrial plant: simulation tool. Energies 2020;13(15):3807.
[68] Amran UI, Ahmad A, Othman MR. Kinetic based simulation of methane steam reforming and water gas shift for hydrogen production using aspen plus. Chem Eng Trans 2017;56:1681–6.
[69] Xu J, Froment GF. Methane steam reforming, methanation and water-gas shift: I. Intrinsic kinetics. AIChE J 1989;35(1):88–96.
[70] Nikooyeh K, Jeje AA, Hill JM. 3D modeling of anode-supported planar SOFC with internal reforming of methane. J Power Sources 2007;171(2):601–9.
[71] Saebea D, Authayanun S, Patcharavorachot Y. Performance analysis of direct steam reforming of methane in SOFC with SDC-based electrolyte. Energy Rep 2020;6:391–6.
[72] Aguiar P, Adjiman CS, Brandon NP. Anode-supported intermediate temperature direct internal reforming solid oxide fuel cell. I: Model-based steady-state performance. J Power Sources 2004;138(1–2):120–36.